Environmental Science Processes & Impacts

ROYAL SOCIETY OF CHEMISTRY

PAPER

View Article Online
View Journal

Cite this: DOI: 10.1039/d6em00126b

Release of microplastics and metals from antifouling paint during weathering in simulated cold climates

Guadalupe Santos, [a] Georgina C. Kalogerakis,[a] Jun-Ray Macairan,[a] Laura M. Hernandez, [a] Houssame-Eddine Ahabchane,[b] Jennifer F. Provencher,[c] Kevin J. Wilkinson *[b] and Nathalie Tufenkji *[ad]

Marine antifouling paints are often overlooked as a source of microplastic pollution in the aquatic environment even though they may release microplastics and metals, including metallic nanoparticles, into the environment, especially following exposure to environmental stressors. Notably, photodegradation *via* sunlight and seasonal freeze-thaw cycles are impactful weathering processes that can affect boat hulls in cold climates. In this study, steel coupons coated with marine antifouling paint were submerged in water and exposed to three laboratory-controlled weathering treatments, namely, UV irradiation (UV), freeze–thaw (FT), and UV irradiation combined with freeze-thaw (UV-FT) over 42 days. Water samples were analyzed using optical photothermal infrared spectroscopy (O-PTIR), inductively coupled plasma mass spectrometry (ICP-MS), single particle ICP-MS, and microscopic imaging in order to quantify microplastics, metals and inorganic nanoparticles released from the painted surfaces. Weathering treatments released microplastics through photochemical degradation (UV) and ice abrasion. Meanwhile, for heavy metals, Cu was dominantly released in its microplastic-bound form and Zn in its dissolved form. UV-exposed paint likely underwent oxidative degradation, whereas FT exposure likely caused damage *via* ice abrasion, resulting in the production of paint microplastics in both cases. The IR and Raman signals showed that paint microplastics generally had high similarity to their respective painted coupons, except for the UV treatment, indicating that paint microplastics can be traced to their original source. Of the three treatments, the combined treatment of UV and FT released the highest concentrations of Cu and Zn over 42 days (49 000 ± 20 000 μg g^{-1} and 14 000 ± 7000 μg g^{-1}, respectively). Cu was released at higher concentrations under weathering conditions that involved abrasion (*i.e.*, UV-FT and FT). In contrast, more Zn was measured in the UV, HC, and CC treatments. Our findings provide a better understanding of the mechanisms leading to the release of paint-derived contaminants into the environment and further highlight the risks posed by the extensive use of marine antifouling paints.

Received 17th February 2026
Accepted 5th April 2026

DOI: 10.1039/d6em00126b

rsc.li/espi

Environmental significance

Marine antifouling paints release microplastics and metals into the environment following their degradation after exposure to environmental stressors. However, analytical data on the release, behaviour and transformations of these paint-derived contaminants is still lacking, especially in relevant environmental contexts. By mimicking stressors such as sunlight, temperature fluctuations, and freeze–thaw cycles under controlled conditions, we gain a better understanding of how paint microplastics, dissolved metals, and metal nanoparticles are released from painted surfaces. Because these contaminants can follow multiple pathways in environmental and biological systems, determining their environmental fate and impact is essential to improving monitoring and supporting mitigation strategies for paint-derived pollution.

Introduction

The global demand for paint reached 52 million tonnes in 2019, with the maritime industry being one of the major sectors that heavily rely on paint and coatings.[1,2] Marine paints are applied to the surfaces of structures and vessels (*e.g.*, boats, ships, trawlers) that are regularly exposed to water to prevent the growth of sessile organisms or biofouling.[3] For example, since biofouling can affect vessel performance and fuel usage *via*

[a]*Department of Chemical Engineering, McGill University, Montreal, Quebec, H3A 0C5, Canada. E-mail: nathalie.tufenkji@mcgill.ca*

[b]*Department of Chemistry, University of Montréal, Montreal, Quebec, H2V 0B33, Canada. E-mail: kj.wilkinson@umontreal.ca*

[c]*Environment and Climate Change Canada, National Wildlife Research Centre, 1125 Colonel By Drive, Ottawa, Ontario, K1A 0H3, Canada*

[d]*United Nations University Institute for Water, Environment and Health, Richmond Hill, Ontario, L4B 3P4, Canada*

increased drag,[4] antifouling paint is regularly applied to boat hulls. Antifouling paint formulations are typically made up of a polymer backbone consisting of alkyds, acrylic, or polyurethane; plasticizers; and solvents.[5,6] Inorganic components are also incorporated into paint, like additives (*e.g.*, biocides, surfactants, anticorrosion agents) and pigments.[7] Nonetheless, when marine paints are exposed to a range of environmental stressors (*e.g.*, UV irradiation, wind, abrasion), the polymeric binder can degrade, generating paint particles that include microplastics, nanoplastics and metallic nanoparticles.[4,6,8–10] Indeed, some antifouling paints are designed to undergo controlled degradation of their polymeric binders to expose a surface with higher biocidal concentration (*i.e.*, self-polishing paints).[3,11] This process can produce paint microplastics. As such, paint microplastics have been found in a variety of environmental matrices, including oceans, coastal waters, estuaries, lakes and sediments.[8,12–17] For example, in one study, alkyd and epoxy plastics from paints were the second most abundant microplastic type found in the Atlantic Ocean.[8]

Paint microplastics are different from many other microplastics in that they generally contain high concentrations of metals that are used as pigments or additives, such as biocides. In the case of antifouling paints, copper (Cu) and zinc (Zn) are often included in the formulations of metal biocides.[18] Accordingly, high levels of metal biocides are frequently detected in marine waters and sediments close to high traffic areas and maintenance facilities,[19–21] with dissolved Cu levels reaching up to 21.0 μg L^{-1} and dissolved Zn up to 9.96 μg L^{-1} in sea surface water.[22,23] In sediments, concentrations can reach up to 19.46 μg g^{-1} and 148.48 μg g^{-1} for Cu and Zn, respectively.[24] The U.S. Environmental Protection Agency's water quality criteria, based on the Biotic Ligand Model, recommend chronic exposure limits of 0.83 μg L^{-1} for Cu and 0.946 μg L^{-1} for Zn in order to protect marine life, although levels measured near marinas may exceed this threshold.[25] While it is well recognized that metals released from paints can detrimentally affect the function and behaviour of organisms,[17,26–28] Cu and Zn are still used as "less toxic" alternatives to banned biocides such as organotin.[29]

There is limited literature demonstrating the release of diverse contaminants (*i.e.*, microplastics, nanoplastics, metals, and metallic nanoparticles) from marine or commercial paints (Table S1). Indeed, our understanding of the release, behaviour and initial transformations of paint-released materials after exposure to physical and chemical stressors in the environment remains incomplete, due in large part to a lack of established analytical approaches to measure the released contaminants (Table S1). Simon *et al.* (2021) found that the chemical structure of the polymer binder in microplastics generated from marine antifouling paints was altered after exposure to UV-C irradiation.[30] These changes included a higher surface area and increased hydrophilicity due to the generation of new functional groups in the binder. Furthermore, the metal forms released from paints are still largely uncharacterized. Although several studies report that metals are leached from painted surfaces, only a few studies specify whether they are released as bulk materials, nano- or colloidal particles or dissolved forms. For example, a study conducted by Miller *et al.* (2017) revealed that Cu from an antifouling paint formulation was mainly released in its dissolved form, with the nanoparticulate Cu fraction constituting a maximum of 13.7% of the total Cu released over 120 days.[18]

The effects of environmental parameters on the rate of metal leaching from paints have also been studied. For example, Singh and Turner (2009) observed increased leaching of Cu and Zn with decreasing temperature from antifouling paint particles submerged in water.[31] They attributed the observed losses to complex reaction kinetics and the presence of dissolved calcium carbonate, which may be included as a component in the paint. Furthermore, paint type and composition can also influence leaching rates. For example, acrylic-based paints were shown to release higher concentrations of metallic biocides as compared to epoxy- and resin-based paints, a result that was attributed to higher hydrolysis rates.[32] So-called biocide-free paints were also found to release higher levels of Zn (4.4–8.2 μg per cm per day) compared to biocide-containing leisure boat paint and ship paints (3.0 μg per cm per day and 0.7–2.0 μg per cm per day, respectively).[33] This is concerning since biocide-free paints are advertised as controlling biofouling *via* erosion and not by metal release.

Although these studies provide valuable insight on the release, behaviour and initial transformations of paint-derived contaminants following weathering exposure, there is a scarcity of literature on the nature or effects of multiple environmental stressors acting simultaneously. In real settings, marine paints may be subjected to complex environmental stressors, such as UV exposure, temperature fluctuations and freeze–thaw cycles. Understanding how these factors act together to influence microplastic release, metal leaching and the behaviour of paint-derived contaminants remains a significant knowledge gap in the field. Previous literature has shown that paint-derived microplastics and associated metal additives are highly toxic to aquatic organisms, inducing physiological stress, reduced growth and impaired reproduction.[27,34,35] High mortality has also been observed when organisms were exposed to antifouling paint particles.[17,27] Given their potential toxicity and the propensity of their forms to change over time, it is necessary to determine the major physicochemical factors driving the entry of these paint-derived contaminants into aquatic systems. However, even as concerns over the environmental risks associated with paints continue to grow, no study to date has simultaneously quantified and characterized microplastics, metals and metal nanoparticles released from antifouling paint under environmentally relevant weathering processes. Additionally, the effects of photodegradation and freeze–thaw cycles remain poorly understood. Accelerated UV-C radiation has been shown to degrade paint binders, altering the physicochemical properties of antifouling paints and increasing metal leaching,[30] while freeze-thaw cycles can induce surface fracturing, weaken polymer matrices and promote the release of metals from paints.[36,37] To our knowledge, this is the first study to simultaneously assess the release of paint microplastics, dissolved metals, and metal nanoparticles under environmentally relevant weathering conditions. Previous studies have analyzed these contaminant types separately and the combined effects of UV and freeze-thaw cycles on paint degradation have not been

explored. We hypothesized that UV exposure would promote the oxidative degradation of the antifouling paints, whereas the freeze-thaw cycling would primarily mechanically abrade the material, thus producing distinct release characteristics for paint-derived microplastics. For metallic contaminants, we hypothesized that under weathering conditions, metal concentrations bound to the paint microplastics and the dissolved fraction would increase with time and that nanoparticle concentrations would subsequently decrease due to agglomeration or dissolution. We tested these hypotheses by placing painted steel coupons in a simplified aqueous matrix where they were exposed to controlled weathering processes (UV irradiation, freeze-thaw cycles, and a combination of the two) and corresponding temperature controls (high temperature and cold temperature) to give us a better understanding of the mechanisms that drive contaminant release. This study will provide an initial assessment of the release of microplastics, metals and metal nanoparticles from antifouling paints under these environmentally relevant weathering scenarios. Specifically, we aimed to: (i) quantify and characterize microplastics, metals, and metal nanoparticles released from painted surfaces; and (ii) identify and examine the possible mechanisms driving contaminant release under simulated UV and freeze-thaw conditions relevant to cold climates.

Materials and methods

Coupon preparation and paint application

Coupons (7.62 cm long × 6.35 cm wide × 0.19 cm thick) were cut and deburred from a large low carbon steel plate (catalog #6544K56, McMaster-Carr), following the guidelines adapted from ASTM D3623-78a.[38] The coupons were sanded using 80-grit sandpaper before being coated on both sides with four layers of epoxy primer (InterProtect 2000E, Interlux®) using a natural hog brush. Excess paint from each layer was removed with an applicator (Bird Film Applicator®, Inc, Washington, USA) to achieve a wet film thickness of 0.01 cm. After drying of the primer, two layers of antifouling paint (MicronCSC-CA, Interlux®) were applied using the same procedure. The final layer of paint was left to dry for at least 24 h before any water exposure, achieving a dry film coating with a thickness between 0.01 and 0.02 cm, in accordance with ASTM guidelines.[39] The coupons were weighed before and after application of each type of paint to determine the mass of applied paint, which was, on average, 4.39 ± 0.27 g of primer + antifouling paint per coupon. Although coupons painted with only primer are uncommon in practical applications, they were included to establish a baseline performance of only the primer and to isolate the influence of the antifouling paint. Uncoated steel coupons were included in our initial setup but released atypical particles. Thus, primer covered coupons were the best control to characterize contaminant release from the antifouling paint.

Experimental setup

Each coupon was placed in a pre-weighed 500 mL clean glass jar (Fisher Scientific) filled with 270 mL of demineralized water, which was then covered with a pre-cleaned glass Petri dish (Fisher Scientific). Demineralized water (resistivity >18.2 MΩ cm; total organic carbon <5 μg C L^{-1}) used in the weathering experiments was obtained from a Direct-Q™ 5 UV water purification system (Millipore Sigma). Demineralized water was used to prevent analytical interferences from salts, ions and organic matter, as this could complicate both microplastics identification and metal and metal nanoparticle quantification. For each weathering treatment, two types of coupons were tested: (i) coupons with only four layers of the primer and (ii) coupons with four layers of primer and two layers of antifouling paint (Fig. 1). A non-painted coupon was not tested due to high metal concentrations (and degradation of the surface) observed in preliminary experiments.

Three weathering treatments were performed: (i) UV irradiation (UV), (ii) freeze-thaw (FT), and (iii) a combination of freeze-thaw and UV irradiation (UV-FT). In addition, two controls were included: (i) a cold control (CC) and (ii) a hot control (HC) in order to provide baseline data for temperature effects that may have resulted from the UV lamp (explained below). The UV treatment was carried out in a custom-made metal chamber equipped with reptile lamps (Arcadia 54w T5 D3+ 6% UVB 46″, ReptilesRuS). For the UV treatment, the lamps were turned on and off every 24 h for 42 days, resulting in 21 UV cycles. During the UV exposure, the temperature in the chamber reached 30.3 ± 0.8 °C, while it was 22 ± 0.5 °C when the UV lights were turned off. To account for these temperature fluctuations and better understand the contribution of UV irradiation, we added an additional control (HC), where samples were kept in an incubator (no UV irradiation, Multitron Pro, Infors HT) that was cycled (24 h) between 30 °C and 22 °C for 42 days. For the FT treatment, coupons were placed in a freezer (−10.4 ± 3.8 °C, Samsung) for 24 h and then placed in a refrigerator for thawing (5.7 ± 2.1 °C, Samsung) for 24 h over 42 days (21 FT cycles). For UV-FT treatment, the coupons were exposed to UV light for 24 h and then placed in the freezer for 24 h, which also resulted in 21 UV-FT cycles. Both photosynthetic flux (or PAR, 400–700 nm) and UV radiation were measured to provide a realistic representation of natural solar irradiance. Assuming an average UV irradiance of 12.7 ± 1.0 W m^{-2} (or 145 ± 11 μmol m^{-2} s^{-1}) for 21 days when the UV was on, the resulting cumulative UV exposure in the weathering experiments was 6401 W h m^{-2} or 47.7 days of natural radiation in Canada, following Hernandez *et al.* (2023) (see Text S1 for calculations).[40] For CC, coupons were placed in the refrigerator (5.7 ± 2.1 °C, Samsung) for 42 days. For weathering treatments involving UV, UV radiation and photosynthetic flux were measured at the bottom of the jars with the appropriate meters (*i.e.*, Apogee MU-200 UV meter and Apogee MQ-100 Quantum Integral Sensor, respectively). For UV-FT experiments, samples were first acclimatized in the refrigerator for 30 to 60 min before every FT 24 h cycle and before every UV 24 h cycle in order to minimize jar breakage from temperature changes. Each set of experimental conditions was examined in triplicate, with samples collected from each jar at predetermined time points.

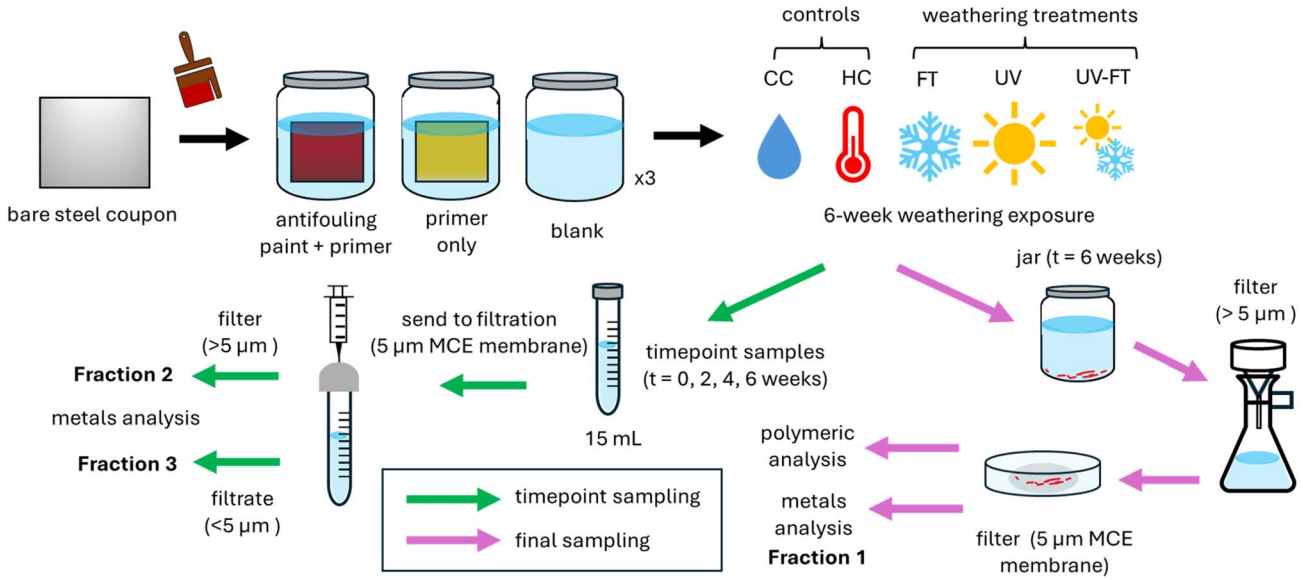

Fig. 1 Overview of the experimental setup including sampling and chemical analyses. The samples were divided into three fractions: Fraction 1 (sedimented paint microplastics consisting of >5 µm particles recovered from the bottom of the jar); Fraction 2 (suspended paint microplastics >5 µm); and Fraction 3 (microplastics, nanoparticles & dissolved metals <5 µm).

Sampling of weathered paint samples

Before the coupons were exposed to the various weathering treatments, 15 mL of water from each jar was collected with a 5 mL plastic pipette pre-rinsed with demineralized water. Further aliquots (timepoint samples) were collected every 14 days up to a maximum of 42 days during the weathering experiments. Namely, 15 mL of the water was sampled every 14 days in a sterile plastic tube (Corning Falcon) for metal analyses. To account for evaporation and water removed for sampling, the weights of the jars were continuously monitored, and an appropriate volume of demineralized water was replenished immediately following sampling (every two weeks). Samples were refrigerated until analysis. At the end of the 42 days, the coupons were removed from the jar using a clean nitrile glove. The jars were then covered with PTFE-lined polypropylene caps (Fisher Scientific) and stored in the refrigerator until further analysis. The jars were not sonicated since preserving the final, undisturbed state of the released particles was necessary for optical microscopy analysis of the paint microplastics.

Size separation of paint samples

The paint samples were divided into size fractions for the analysis of microplastics, metals, and nanoparticles (Fig. 2).

Samples remaining in the jars at the end of the 42 day weathering exposure were filtered using a glass vacuum filtration system (Sigma-Aldrich) in a BSC. A mixed cellulose ester (MCE) membrane filter (diameter 47 mm, pore size 5 µm; MF-Millipore™) was placed in the filtration system and washed 3× with demineralized water. MCE membrane filters were selected because their hydrophilic nature allows micron-sized particles to be efficiently retained and they are widely used in filtering high-particulate water samples. Then, the entire jar volume (~150 mL) was filtered. Using plastic tweezers, the filter was placed in a clean glass Petri dish labelled with a 100-square grid (Fisher Scientific) and allowed to dry in the BSC. The material trapped on this filter is referred to as Fraction 1 (Fig. 2). Between samples, the filtration system was washed thoroughly with demineralized water and acetone in order to minimize any potential cross contamination between samples.

The plastic tubes containing the timepoint samples were first sonicated for 30 min in a sonicator bath (Branson Ultrasonics, model CPX) and then the samples were filtered through a 5 µm filter that resulted in two fractions: (i) Fraction 2 (F2): retained particles >5 µm in size and (ii) Fraction 3 (F3): filtrate with particles <5 µm in size (Fig. 2). Filtration was performed

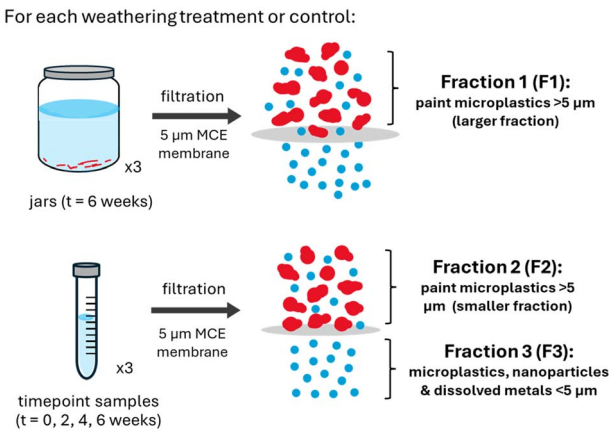

Fig. 2 Size fractions obtained for timepoint samples (t = 0, 2, 4 and 6 weeks) and jar samples (6 weeks). Fraction 1 (F1), Fraction 2 (F2) and Fraction 3 (F3) were filtered over a 5 µm membrane. Samples were collected in triplicate. Fraction 1 includes the larger particles that sedimented to the bottom of the jar while Fraction 2 consists of the suspended particles that are larger than 5 µm.

using an MCE membrane filter (25 mm diameter, pore size 5 μm; MF-Millipore™) that was placed in a polypropylene filter holder (Cole-Parmer). The filter was first pre-rinsed with 12 mL of demineralized water and pre-conditioned with 6 mL of sample. Four to 9 mL of the sample was then filtered, and this filtrate (F3) was collected in 15 mL polypropylene Falcon tubes. Filters with retained particles were placed into empty 50 mL Falcon tubes using plastic tweezers (Fisher Scientific).

Chemical analyses

Detection of nanoparticles using SP-ICP-MS in F3

The presence of metal nanoparticles in the filtrates of each timepoint sample (F3) was evaluated using single particle inductively coupled plasma mass spectroscopy (SP-ICP-MS).[37] A multi-quadrupole ICP-MS (NexION® 5000 Series ICP-MS, PerkinElmer) was used to measure Cu-containing nanoparticles in F3. Zn-containing particles were also detected but the dissolved signal was very high, leading to very high size detection limits. For particle size determinations, the composition and density (6.0 g cm^{-3}) were assumed to correspond to cuprous oxide (Cu_2O), since this is one of the main antifouling agents in the paint. ^{63}Cu was calibrated using ionic standards that were prepared from a concentrated stock solution (Inorganic Ventures IV-ICPMS-71A) in the range of 0.05–30 μg L^{-1}. Samples were analyzed for 50 s using a dwell time of 100 μs. Transport efficiency (TE) was determined using 50 nm gold (Au) ultra-uniform nanoparticles (NanoComposix, San Diego, CA, USA) and ranged from 4.27% to 5.63%, depending on the analysis day. Ag nanoparticles (60 nm) were used to validate the TE. Filtered samples were diluted 3–50 times, as required, in order to limit particle coincidence. Data were processed using the Syngistix software (PerkinElmer) and validated using SPCal.[41] Organization of the large dataset was achieved using R software and ChatGPT. Samples with <200 particle events (measured over 50 s) were deemed statistically insignificant and were excluded from further calculations.

Imaging of paint microplastics >5 μm in F1

Particle morphologies and particle numbers were determined in the filter retentates of the final (6 week) jar samples (F1) using a stereomicroscope (Olympus, model SZX16). At least 30 representative images were taken for each sample, over an estimated area of 480 mm^2. Particle sizes were determined by using a ruler as a reference and by analyzing the images with ImageJ (version 1.54 g).

Analysis of the painted coupons and microplastics in F1 with mIRage®

The polymeric composition of the weathered, painted coupons and paint microplastics in F1 was determined using optical photothermal infrared spectroscopy (O-PTIR) using the mIRage® IR microscope (Photothermal Spectroscopy Corp.). Imaging was performed directly on the painted coupons, whereas for the paint microplastics, imaging was done on the filter. To minimize burning of the microplastics and to obtain a high intensity signal, an avalanche photodiode detector was utilized in the analysis. Three arbitrary fields of view, where microplastics and agglomerates could be seen, were selected. In each field of view, at least nine IR spectra from arbitrary individual particles were acquired (2998–2688 cm^{-1} and 1798–940 cm^{-1}).

A Pearson correlation coefficient was used to compare the treatments and controls against the reference, untreated antifouling paints.[30,42,43] This coefficient measures the strength and direction of a linear correlation between two different sets of data. It can be between −1 for a perfect negative correlation and 1 for a perfect positive correlation, with a value of 0 indicating no relationship.

Contact angle measurements of paint coupons

In order to evaluate the wettability of the weathered coupon surfaces, the static water contact angle was measured. Measurements were performed using a drop shape analyzer goniometer (DSA20E, Krüss) equipped with a high-resolution camera and controlled using the Advance software (version 1.16.010201). A 1 mL syringe with a fine-gauge needle was filled with LC-MS grade water and mounted on the automated dosing system. Using the sessile drop method in the Advance software, a 2 μL droplet was dispensed onto the sample surface. The contact angle was immediately measured and calculated automatically from the drop profile at the liquid–solid–air interface. Each sample was measured in triplicate at three different locations across the surface. For the UV-FT coupons, most of the first layer of antifouling paint had flaked off, exposing the second layer of antifouling paint underneath. Therefore, triplicate measurements were done for the first layer of paint that remained, as well as for the second layer of paint. All measurements were performed at room temperature and contact angle values are reported as mean ± standard deviation. The contact angles were compared using the Mann–Whitney *U* test.

Metal analyses of F1, F2 and F3

All three fractions (F1, F2 and F3) were analyzed for ^{63}Cu and ^{66}Zn concentrations using a multi-quadrupole ICP-MS (NexION® 5000 Series ICP-MS, PerkinElmer). For F1 and F2, filters were placed in 50 mL polypropylene Falcon tubes and then digested with aqua regia. Aqua regia was used since it is both a widely used digestion method for paints,[31,43–46] and it can yield up to 95% recovery for Cu and 100% recovery for Zn in complex matrices like soil.[47]

For F3, filtrate samples were acidified with 2% v/v ultrapure nitric acid (PlasmaPURE Plus, Analytichem) for 24 to 48 h. Procedural blanks were also prepared, digested and analyzed. F1 and F2 samples were diluted to 4% v/v acid before analysis, with additional dilutions performed, if required. As above, Cu and Zn were calibrated using standards made up from IV-ICPMS-71A (Inorganic Ventures) and diluted to 0.05–30.00 μg L^{-1} in 2% nitric acid. Standards (Analytichem Quality Ctrl. Std. 4 and High Purity Standard 27 Component ICP Standard) were used to ensure quality control. In order to account for

contamination, concentrations from the procedural blanks were subtracted from the measured sample concentrations.

Quality assurance for weathering experiments and chemical analyses

Glassware was first cleaned three times with low foaming soap (Alconox® detergent, Millipore Sigma) and then rinsed three times with demineralized water. Subsequently, it was cleaned three times with acetone (C_3H_6O, ≥99.5%, Fisher Scientific) in a biological safety cabinet (BSC) and left to dry overnight. All subsequent sample handling, drying, and filtration were also done in a BSC to minimize airborne particle contamination. Although some plastic consumables were used for routine laboratory handling (*e.g.*, polypropylene tubes and pipette tips), these materials were visually and morphologically distinguishable from paint microplastics. The plasticware used was transparent and smooth, whereas paint microplastics were irregularly shaped, had a rough surface and were red in colour. Because the weathering experiments were conducted in a closed system containing only the painted coupon, the only visible materials that could be generated were paint fragments, or less commonly, iron particulates from the exposed metal coupon. Paint microplastics were therefore identified using a two-step approach: (1) visual identification based on the characteristic morphology and colour of the paint fragments; and (2) O-PTIR analysis of a subset of suspect paint particles from each set of weathering conditions to confirm that the fragments were indeed paint. This process ensured that all analyzed particles were correctly identified as paint microplastics. Procedural blanks were also processed alongside other samples to account for possible metal and plastic contamination (Fig. 1).

Though metal nanoparticles could be quantified with SP-ICP-MS, nanoplastics could not be analyzed using the same technique. Nanoscale particles (<1 μm) were detected using Nanoparticle Tracking Analysis (NTA); however, this technique only provides information on size and concentration, not the chemical composition. Since we could not confirm the chemical identity of these particles and given that the results were variable among replicates, we did not report this data in our study.

Results and discussion

Confirmation of the identity of paint microplastics with O-PTIR

The paint that was studied is self-polishing, *i.e.*, the outer layer of the paint is designed to slough off, upon exposure to water. As such, paint microplastics were expected and detected in all samples. For fraction F1 (>5 μm particles collected after 6 weeks of weathering), particles released from the painted coupons were identified and imaged using O-PTIR (Fig. S1). In all weathering treatments and controls, major peaks in the spectra matched with characteristic peaks attributed to the untreated antifouling paint, *i.e.*, the reference paint (Fig. 3A).

An older formulation of the antifouling paint indicated rosin as one of its components, though it is not listed as a component for the current antifouling paint (Table S2). Rosin is a naturally occurring polymer, which can be categorised as a microplastic if chemically altered for a given application, such as paint.[30] Comparing the spectra of the rosin and that of the reference antifouling paint yielded similar major peaks at 2933, 2856, 1652, 1160, and 1038 cm^{-1} (Fig. S2). However, metal–carboxylic acid groups (1585 and 1405 cm^{-1}) were not present in the original rosin, which may indicate the presence of biocides. Peak assignments are shown in Table 1. Additionally, the experimental spectra were found to be similar to those observed for a nautical paint studied by Simon *et al.* (2021).[30] In their study, the paint was also a self-polishing antifouling paint incorporating zinc oxide (ZnO) and Cu_2O as the metal biocides. Indeed, the antifouling paint used in their study contained metal–carboxylic acid groups (1585 and 1405 cm^{-1}), which was not seen in the original rosin binder (Fig. S2).

Based upon the strength of the Pearson correlation coefficient, no obvious spectral changes were found when comparing spectra from the weathered paint microparticles to the

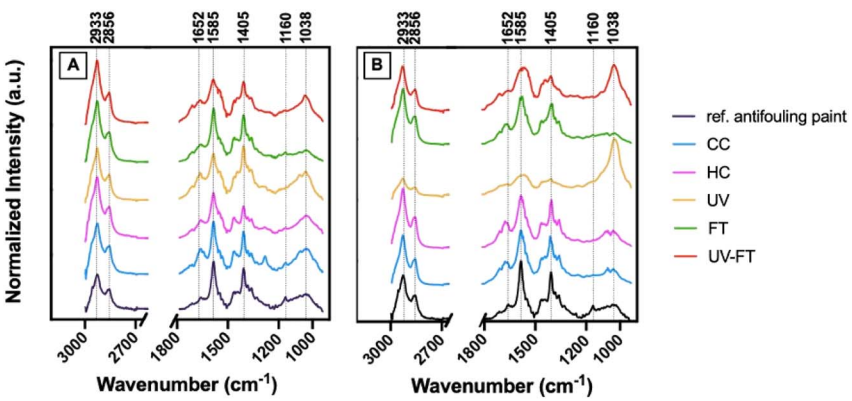

Fig. 3 Averaged normalized spectra from O-PTIR analysis of (A) paint microplastics collected from the water after six weeks of exposure (*i.e.*, F1) and (B) painted coupons following their exposure for six weeks to one of five weathering treatments or controls: (i) CC = cold control; (ii) HC = hot control; (iii) UV=UV irradiation; (iv) FT = freeze-thaw; and UV-FT = UV and FT combination. All spectra were compared to the average normalized spectra of the untreated reference antifouling paint fragments, denoted as "ref. antifouling paint" (black). Common wavenumbers shared among all spectra are labelled on the upper *x*-axis (over the range 3000 cm^{-1} to 940 cm^{-1}).

Table 1 Peak assignments (cm^{-1}) for spectra acquired using O-PTIR for weathered and untreated antifouling paint particles. Assignments are based on Hayes *et al.* (2014), Simon *et al.* (2021) and van der Weerd *et al.* (2005).[30,48,49]

Wavenumber (cm^{-1})	Functional group	Class	Origin
2933	Methylene asymmetric C–H stretch	Alkane	Binder
2856	Methyl symmetric C–H stretch	Alkane	Binder
1652	C=C stretch	Alkene	Binder
1585	Metal carboxylate, asymmetric COO stretch	Carboxylic acid	Binder
1405	Metal carboxylate, symmetric COO stretch	Carboxylic acid	Binder
1160	C=O	Carboxylic acid	Binder
1038	Si-OR	Silicate	Pigment

untreated antifouling paint (Fig. 3A and S3). High positive correlations were calculated for all weathering treatments and controls ($n = 27$ spectra for each set of conditions) when compared to the reference antifouling paint ($n = 9$ spectra): 0.81 $\pm$ 0.21 for CC, 0.92 $\pm$ 0.02 for HC, 0.91 $\pm$ 0.03 for UV, 0.88 $\pm$ 0.03 for FT, and 0.95 $\pm$ 0.02 for UV-FT (Fig. S4 and Text S2).

Chemical changes in the painted coupons observed for the treatments with UV

The physical appearance of the painted coupons was clearly altered after six weeks of weathering, as compared to both control conditions (HC and CC; Fig. S5 and S6). This change in appearance was also reflected in the IR spectra, which indicated important chemical changes, especially for the UV and UV-FT treatments (Fig. 3B). Furthermore, the paint on the weathered coupons exhibited some important chemical changes, outlined in the next paragraph, when compared to the untreated antifouling paint, especially for the UV and UV-FT treatments (Fig. 3B). When compared to the reference paint, Pearson correlation coefficients of 0.91 $\pm$ 0.03 were found for CC, 0.91 $\pm$ 0.02 for HC, 0.28 $\pm$ 0.18 for UV, 0.92 $\pm$ 0.01 for FT and 0.69 $\pm$ 0.25 for UV-FT (Fig. S7).

Images obtained using O-PTIR confirmed that the coupons exposed to UV irradiation had smoother surfaces as compared to the controls and FT treatment (Fig. S6). Higher water contact angles were found for the surfaces of coupons exposed to the UV-FT treatment (mostly for the first layer, which was exposed longer) and the UV only treatment when compared to the controls and the FT treatment. This could be associated with chemical changes, making the surfaces more hydrophobic (Fig. S8 and Table S3).[50] Chemical changes, subsequent to the UV and UV-FT exposure, were confirmed by the broadening of several of the characteristic peaks in the O-PTIR spectra (Fig. 3B). UV irradiation is known to accelerate chemical reactions in materials and cleave some chemical bonds (primarily C–H and C–O).[51] UV exposure can also promote oxidation, leading to the formation of hydroxyl groups within the unsaturated groups of paint binders.[30,52] Indeed, the peak at 1652 (indicative of alkene groups), and peaks at 1595 and 1405 cm^{-1} (indicative of metal carboxylate groups), lost their sharpness in the antifouling paint coupons that had been exposed to UV and UV-FT. This observed broadening is consistent with the formation of hydroxyl groups on the unsaturated sites, corresponding to a degradation of the polymer material. Methylene groups (2933 and 2856 cm^{-1}) in the UV and UV-FT treatments were also found to have broadened, which can be attributed to losses of volatile organic compounds and degradation products from the rosin binder.[52]

Compared to the painted coupons, the paint microplastics recovered from the solutions did not appear to exhibit noticeable chemical changes. We speculate that the paint microplastics released from the coupon surface may have been shielded from UV irradiation by the coupon itself. Indeed, when comparing the released microplastics to the painted coupons, the UV exposed coupon had the lowest similarity to the paint microplastics, regardless of the type of treatment (Fig. S9 and Table S4). Also, the O-PTIR spectra of the UV-exposed coupons indicated weakening of the polymer structure *via* UV-induced oxidation that can result in the generation of paint microplastics.[30,53] Although the UV-FT results in Table S4 suggest the opposite effect, in which cold temperatures from the freeze-thaw cycles may have reduced the oxidizing effect of the UV irradiation, freeze-thaw conditions can still cause shedding of paint microplastics through mechanical means, thus contributing to microplastic pollution from the paint.

Detection of paint microplastics in F1

Paint microplastics were detected in all F1 samples that were collected after six weeks of weathering, including the controls (Fig. 4A). The numbers and sizes of the microplastics were determined for each treatment, except for the UV-FT treatment (Table S5). In that treatment, it was not possible to determine particle counts since the filter was fully saturated with microplastics. The UV-FT condition clearly generated the most particles, followed by the FT, where an average of 67 $\pm$ 30 particles per mL were detected (Fig. 4B). For the UV treatment, microplastic counts (14 $\pm$ 10 particles per mL) were barely higher than what was observed for the controls (6 $\pm$ 6 and 2 $\pm$ 3 particles per mL). That being said, most of the particles that were found in the procedural controls did not have a similar morphology to what was observed in the treatments (UV-FT, FT, UV).

Larger paint microplastics were more prevalent under conditions involving FT cycles (Fig. 5). While it was not possible to confidently determine particle counts for the UV-FT treatment, we were able to estimate particle sizes since the paint

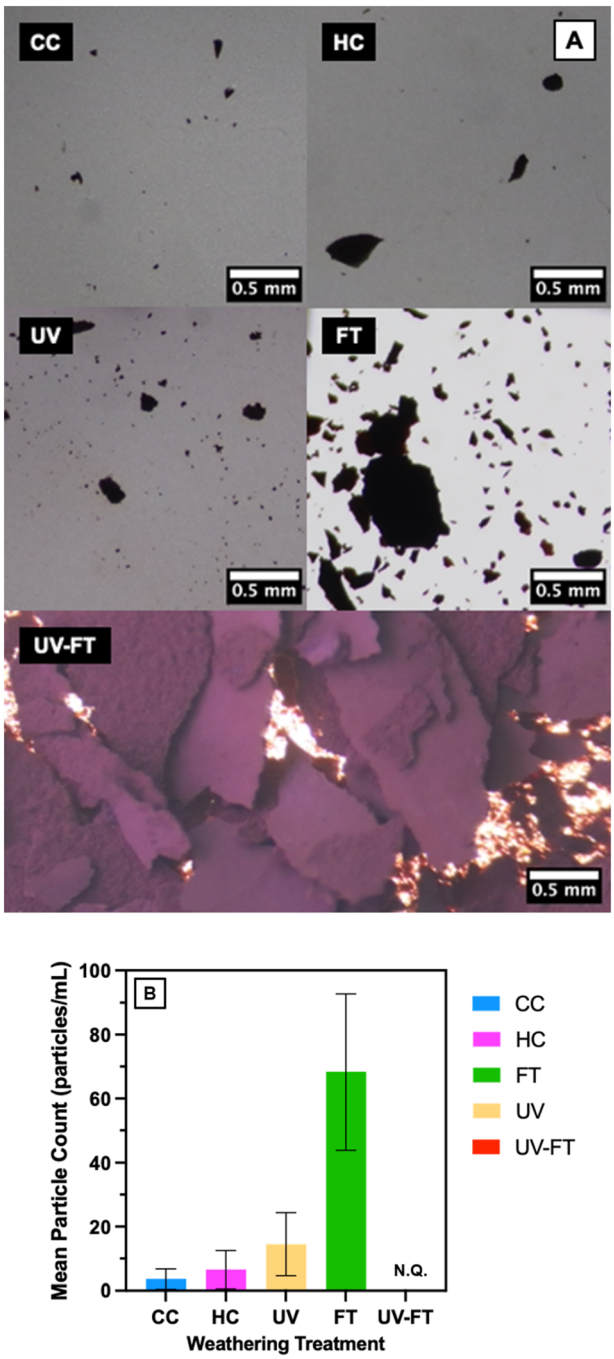

Fig. 4 (A) Optical microscope images of paint microplastics released from controls (*i.e.*, CC = cold control, HC = hot control) and weathering treatments (*i.e.*, UV=UV irradiation, FT = freeze-thaw, and UV-FT = UV and FT combination) and (B) Bar graph showing the mean particle count (particles per mL ± SD) released from the controls and weathering treatments. For UV-FT, N.Q. indicates that particle counts could not be quantified due to an oversaturation of the filter with paint microplastics.

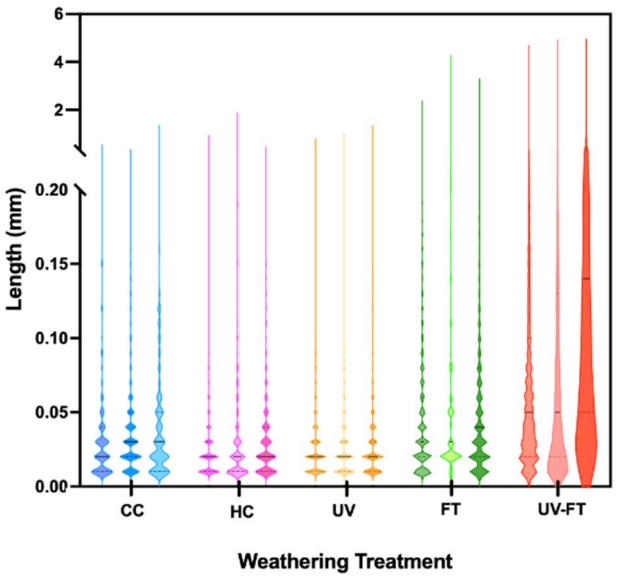

Fig. 5 Violin plots of the size distributions of paint microplastics released from the temperature controls and weathering treatments (CC = cold control, HC = hot control, UV=UV irradiation, FT = freeze-thaw, and UV-FT = UV and FT combination). The size distribution for each individual triplicate sample is shown. Dashed lines indicate the quartiles and the solid black lines indicate the median.

microplastics could be individually manually sized. The largest paint microplastics were detected in the UV-FT treatment as compared to all other treatments and controls (maximum size 4.8 ± 0.1 mm with an average mean size of 0.20 ± 0.10 mm, Table S4). This was followed by FT (maximum size in the replicates 3.3 ± 1.0 mm; mean size in the replicates 0.07 ± 0.02 mm; Table S4). Measured paint microplastics from the other treatments and controls did not exceed 1.1 ± 0.7 mm (maximum particle size for HC). Freeze-thaw cycles can abrade a material *via* ice abrasion by: (i) creating cracks *via* tensile stress, which can be exacerbated by the seeping of water into cracks that can be frozen again, (ii) releasing fragments that can be dragged onto the original material's surface by the ice, and (iii) hydraulic pressure encouraging fracturing within surface defects of the material.[54] For standing painted marine structures in the tidal zone, such as concrete structures, FT cycles can happen frequently.[55] However, many boats are stored during the winter, at a height at which FT cycles occur frequently. As such, the generation and release of paint microplastics can be delayed. Boats stored in slipways and hard standings are likely to generate fewer paint microplastics as result of FT; however, they still could be deposited onto the ground at which time spring surface runoff could transport them into the aquatic environment.[56,57]

Temporal release of copper and zinc from the paint

Given that Cu_2O and ZnO are the biocidal ingredients in the paint (Table S2), Cu and Zn were measured in F2 (microparticles) and in F3 (5 μm filtrate) (Fig. 6). The UV-FT treatment consistently released the most Cu and Zn from the paints. At the final timepoint (6 weeks), 17.0 ± 3.0 mg g^{-1} of Cu and 6.7 ± 2.0 mg g^{-1} of Zn were released during the UV-FT treatment (Fig. 6A and B). These concentrations are lower than those observed in a previous study that found extremely high concentrations of 400 mg g^{-1} Cu and 250 mg g^{-1} Zn collected

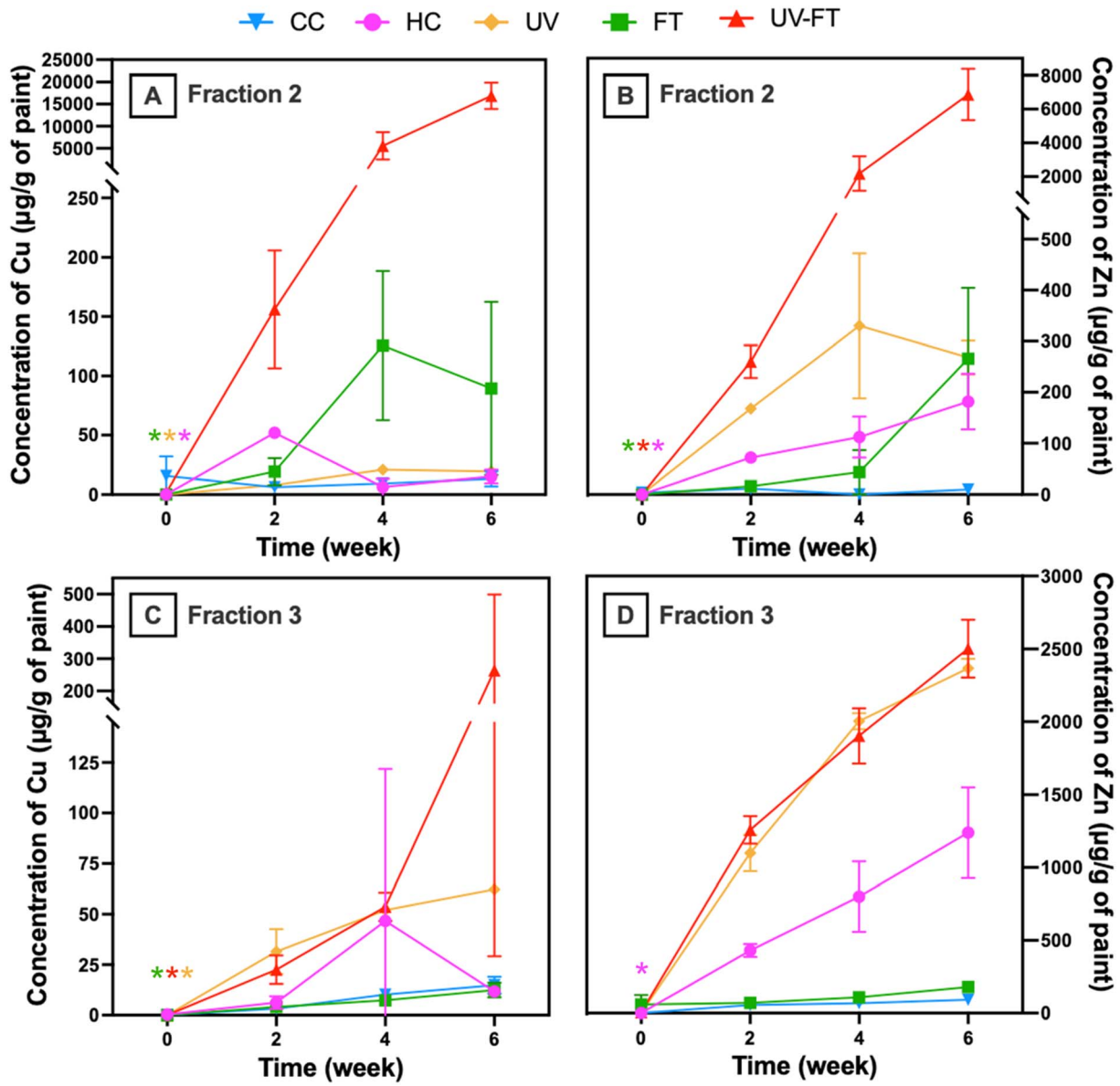

Fig. 6 Total Cu (left) and Zn (right) concentrations released from antifouling painted coupons, in µg g^{-1} of dry paint, from three weathering treatments and two controls in F2 (>5 µm; A and B) and F3 (<5 µm; C and D). Concentrations were normalized to initial paint masses. Error bars denote the standard deviation around the mean for triplicate samples. Asterisks with their appropriate treatments denote values that are below the limit of detection and have been attributed values of LOD/2.

from a boat maintenance facility and attributed to paint microplastics.[58] The results are nonetheless consistent with the field study given that this study looked at relatively short-term (controlled) laboratory exposures.

The high metal concentrations measured in F2 for the UV-FT treatments were consistent with the high concentrations of microplastics that were found for this treatment. For F3, Cu was found at the highest concentration in the UV-FT fraction (260 ± 200 µg g^{-1} of dry paint), followed by UV (62 ± 3 µg g^{-1} of dry paint) whereas the release of Zn was similar for the two treatments (Fig. 6C and D). Indeed, Zn appeared to be more readily leached in its dissolved form than Cu (Tables 2 and 3), similar to previous work on this subject. For example, Jalaie *et al.* (2023) found that ZnO was more readily leached than Cu_2O from antifouling paints that had different polymer binders.[32] Because ZnO has a lower density and a greater solubility compared to Cu_2O, it has a greater propensity to be released as dissolved Zn. As it is liberated, more water may penetrate into the binder, which can in turn dissolve even more ZnO. In Fig. 6D, the HC treatment released the next highest Zn concentrations in F3; however, it should be noted that we observed a decrease in pH in the HC treatment during the six-week exposure (Fig. S10A). Because ZnO dissolves more thoroughly in acidic environments,[59] this may be the cause for the higher Zn leaching in HC. The pH decrease might have been attributed to a more important hydrolysis of the metals,[30] which would be expected at higher temperatures.

Table 2 Masses of Cu per gram of paint released from five different treatments and controls at the 6 week timepoint. Concentrations ± standard deviation (μg of Cu per g of paint) and the sum of each fraction (μg of Cu per g of paint) are shown. The percentage of each fraction with respect to the total mass is also presented

Weathering treatment	F1 (μg g^{-1})	F2 (μg g^{-1})	F3 (μg g^{-1})	F1 + F2 + F3 (μg g^{-1})	F1/(F1 + F2 + F3) (%)	F2/(F1 + F2 + F3) (%)	F3/(F1 + F2 + F3) (%)
CC	11 ± 6	0.050 ± 0.02	15 ± 4	26 ± 9	41.3	0.2	58.5
HC	38 ± 9	0.064 ± 0. 03	12 ± 3	50 ± 10	75.8	0.1	24.1
UV	110 ± 60	0.090 ± 0.01	62 ± 3	170 ± 60	60.5	0.1	39.5
FT	4300 ± 3000	0.35 ± 0.3	12 ± 4	4300 ± 3000	99.6	0.0	0.3
UV-FT	49 000 ± 20 000	72 ± 20	260 ± 200	49 000 ± 3000	99.4	0.2	0.5

Table 3 Masses of Zn per gram of paint released from five different treatments and controls at the 6 week timepoint. Concentrations ± standard deviation (μg of Zn per g of paint) and the sum of each fraction ± standard deviation (μg of Zn per g of paint) are shown. The percentage of each fraction with respect to the total mass is also presented

Weathering treatment	F1 (μg g^{-1})	F2 (μg g^{-1})	F3 (μg g^{-1})	F1 + F2 + F3 (μg g^{-1})	F1/(F1 + F2 + F3) (%)	F2/(F1 + F2 + F3) (%)	F3/(F1 + F2 + F3) (%)
CC	12 ± 20	0.038 ± 0.02	92 ± 30	100 ± 40	10.0	0.0	90.0
HC	11 ± 2	0.77 ± 0.2	1200 ± 300	1300 ± 300	0.9	0.1	99.1
UV	31 ± 17	1.2 ± 0.2	2400 ± 65	2400 ± 70	1.3	0.0	98.7
FT	1300 ± 800	1.0 ± 0.5	180 ± 40	1400 ± 900	85.6	0.1	14.4
UV-FT	14 000 ± 7000	29 ± 8	2500 ± 400	17 000 ± 7000	83.5	0.2	16.4

Forms of copper and zinc released from paint

Cu and Zn concentrations in F3 were initially attributed to the leaching of dissolved metals from the paints. The concentrations of Cu and Zn released from the different weathering treatments and controls are given in Tables 2 and 3 for each of the three fractions for the sample collected at the final (6 week) timepoint. UV-FT released the highest total masses of Cu and Zn (*i.e.*, F1 + F2 + F3). As established above, the UV-FT treatment degraded the surface to the greatest extent.

For most treatments, Cu was mostly released in F1 (large particles), while a majority of Zn was released in F3 (<5 μm) (Tables 2 and 3), demonstrating that Cu was more likely to stay in the paint microplastics, whereas Zn had a higher propensity to be released through leaching, especially for non-abrasive treatments (UV, HC, and CC). Although these results, including the SP-ICP-MS observation of high concentrations of background (*i.e.* dissolved) Zn, suggest that Zn was largely released in dissolved form, Miller *et al.* (2017) showed that Zn could be released from paints in its particulate form (bulk and nanoparticle) in the initial hours of a water submersion.[18] In that case, particulate Zn then quickly dissolved after the first few hours of exposure. Although our data is lacking hour-by-hour concentrations, the decreased pHs measured after two weeks for the UV, HC, CC and UV-FT treatments are consistent with the hypothesis that Zn was mostly present in its dissolved forms in F3 (Fig. S10A).

Release of Cu nanoparticles from the paint

Copper oxide (I), or Cu_2O, nanoparticles have been shown to be released from antifouling paints.[4] Though Cu_2O comprised 30–60% of the total weight of the paint used here (Table S2), the manufacturer did not specifically state if it was added in a nanoparticle form. Measurements by SP-ICP-MS showed clearly that Cu-containing nanoparticles could be detected in F3, for the FT and CC treatments (Fig. S11).

By assuming a spherical shape and density of 6.0 g cm^{-3} corresponding to Cu_2O, we estimate that $1.6 \pm 1.1 \times 10^8$ Cu_2O nanoparticles were released per g of dry paint for the FT-exposed coupons. After four weeks, the number concentration decreased ($4.4 \pm 3.6 \times 10^7$ Cu_2O nanoparticles per g of dry paint) and release was ultimately not statistically significant at six weeks (Fig. S11). Cu_2O nanoparticles were also detected in jars containing CC-exposed coupons, but only at the two-week timepoint ($9.9 \pm 5.6 \times 10^5$ Cu_2O particles per g of dry paint).

The size distributions of Cu_2O nanoparticles generated by the FT treatment could only be determined at two weeks and four weeks. The size distribution of the nanoparticles was found to be similar for both timepoints in the FT treatment, with a mean diameter of 30 ± 1 nm and 29 ± 1 nm for two and four weeks, respectively (Fig. 7). For the CC treatment at two weeks, the Cu_2O nanoparticles were larger in size (average median 61 ± 2 nm). The size range of Cu_2O nanoparticles released from paint is similar to what has been observed in earlier studies. For example, Gondikas *et al.* (2023) reported that the majority of Cu nanoparticles in marinas were approximately 45 nm in size.[10] Similarly, Adeleye *et al.* (2016) observed that 44 nm was the most commonly detected particle size for Cu_2O nanoparticles released from antifouling paints exposed to laboratory-controlled weathering.[4] The larger size distribution in the CC treatment suggests that either the Cu_2O nanoparticles had coalesced or agglomerated or that the freeze-thaw treatment led to greater particle dissolution or simply the extraction of

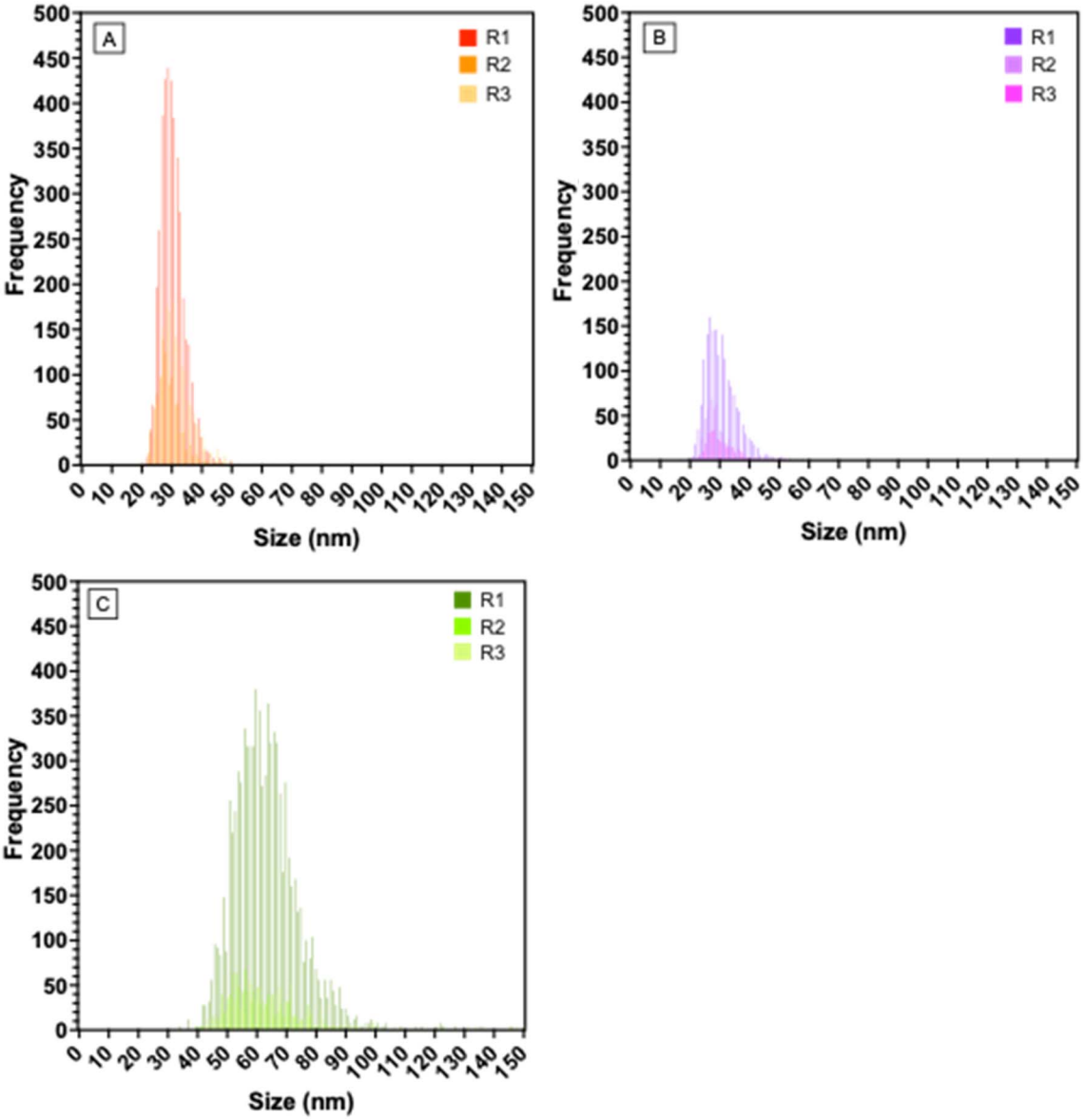

Fig. 7 Size distribution (nm) of Cu_2O nanoparticles released from antifouling paints exposed to (A) the FT treatment after two weeks, (B) the FT treatment after four weeks and (C) CC after two weeks. Bin width is equal to 1 and bin values from 151 to 707 were omitted for clarity. The legend indicates the triplicate samples ($n = 3$) measured for each time point.

smaller nanoparticles. Due to the limited number of samples with significant numbers of nanoparticles, greater precision on the mechanism would be too speculative at this time.

The low detection rates of Cu_2O nanoparticles could be the result of the peak signals (nanoparticles) being overwhelmed by the signal intensity of the dissolved background (raw data provided in Fig. S12). As a reminder, ZnO nanoparticles were also excluded from the data analysis due to the extremely high background, corresponding to dissolved Zn. Although it is possible to reduce the background signal of the soluble metal oxides using ion exchange columns,[60,61] this manipulation was not performed here as the contributions of the dissolved metals were generally much higher than those of the nanoparticles (Table S6). As such, most of the nanoparticle peaks were "masked" by the background, as demonstrated in the raw signal data and consistent with the total metals analysis for F3. Furthermore, a high concentration of Cu was measured in F3 for the UV-FT treatment, indicating that the Cu was either released primarily in its dissolved form or that the nanoparticles dissolved shortly after release (Fig. 6C). Finally, since the UV and HC treatments had relatively high concentrations of Cu in F3 whereas the FT and CC had the lowest concentrations (Fig. 6C) but also the observable nanoparticles, it would appear that heat plays a role in increasing dissolution among the Cu_2O particles.

Limitations

The study has several limitations, which are largely related to the current state-of-the-art of the analytical techniques used for

characterizing nanoplastics, metallic nanoparticles and heterocomposites. Although UV and freeze-thaw processes can fragment microplastics into nanoscale particles, nanoplastic concentrations and sizes could not be confirmed in our study. Although NTA was used to screen particles <1 μm in size, this technique cannot provide chemical identification, and thus we could not discriminate between metal nanoparticles and nanoplastics. Furthermore, the initial particle size distributions of Cu_2O and ZnO could not be determined. Wet, uncured paint cannot be homogeneously dispersed into dilute aqueous suspensions required for SP-ICP-MS, and preliminary experiments resulted in incomplete dissolution and visible phase separation. The manufacturer also did not disclose the particle size distributions of Cu_2O and ZnO; CAS numbers provided no size information. In addition, the exact Cu and Zn content of the antifouling paint was not disclosed—only an estimated range was provided. This prevented precise determination of metal recoveries for this specific paint matrix. Secondly, we could not distinguish between primary and secondary paint-derived contaminants. UV irradiation and freeze-thaw cycling are documented to cause secondary fragmentation of microplastics into nanoplastics.[62] Similarly, metal ions can precipitate to form metallic and metal oxide nanoparticles.[4,18] Thus, differentiating between nanoparticles released from the paint surface from those formed due to fragmentation or re-precipitation of ions remains an important avenue for future work. Thirdly, temporal trends could not be generated for the release of the paint microplastics. In contrast to the analysis of metals and metal nanoparticles, which is performed with little perturbation of the experimental media, microplastic analysis requires large sample volumes. Furthermore, given their sizes, paint microplastics were heterogeneously distributed in the sample containers, with some particles rapidly settling to the bottom of the jar and others adhering to the jar walls and coupon surfaces. Samples taken at intermediate timepoints would have captured only the suspended fraction and not the total microplastic load, leading to inaccurate estimates of microplastic concentrations and sizes. Given the need for large sample volumes, accurate temporal quantification would have required the sacrificial sampling of entire jars at each time point, which was not feasible within the scope of this study. Natural waters contain an assortment of dissolved minerals, salts, and organic matter that can influence paint degradation, metal speciation and release kinetics. In this study, demineralized water was used to minimize contamination and analytical interferences, since salts, ions, and organic matter can hinder both microplastic identification (*e.g.*, O-PTIR and microscopy) and accurate metal or nanoparticle quantification. However, previous literature has shown that the fate, transport and transformation of paint-derived contaminants may differ with pH, salinity, hardness, and total organic carbon content. Finally, the weathering conditions that were examined in this study represented only a subset of environmental stressors encountered by marine paints. While the study focused on UV photodegradation and freeze-thaw cycles, mechanical forces such as wave action and turbulence *via* vessel action, as well as drastic temperature fluctuations, can also contribute to paint degradation in real settings. In addition, the accumulation of biofouling organisms can influence degradation by altering chemical conditions (*e.g.*, pH) and imposing additional mechanical or biochemical stress on the paint surface.[63,64] Incorporating these additional chemical, mechanical and biological stressors into future studies will give a more holistic picture of environmental degradation processes for marine paints.

Conclusions

This study provided the first integrated assessment of microplastics, dissolved metals and metallic nanoparticles released from antifouling paints under UV irradiation, freeze-thaw cycling and a combination of the two. All treatments and controls produced paint microplastics. UV irradiation induced photo-oxidation of the paint binder whereas freeze-thaw cycling likely degraded the painted surface through abrasion, thus aligning with our hypothesis. Exposure to the combined UV and FT treatment appeared to produce a synergistic effect resulting in the generation of the largest and most abundant paint microplastics when compared to each weathering treatment alone. Microplastic release was reported as a single quantity at the end of the 42 day weathering exposure, since large quantities of particles settled quickly in the jars such that a representative sample could not be collected.

Temporal trends in metal release aligned with our predicted behaviour for dissolved and particulate metals. Cu concentrations increased over the 42 day exposure under conditions involving abrasion (*i.e.*, FT and UV-FT), demonstrating the importance of Cu retention in the paint binder and its release with time in the form of microplastics. Zn, in contrast, was released predominantly as dissolved Zn and was most susceptible to UV and heat. Regardless of the exposure conditions, Cu and Zn levels increased over the 42 day exposure period. We also observed the concentrations of Cu nanoparticles decreasing over time; however, dissolved metal concentrations simultaneously became more important, which may have obscured the nanoparticle peaks. These results indicate that copper oxide nanoparticles were present but limited in quantity in this simplified aqueous matrix, potentially due to nanoparticle losses *via* agglomeration or dissolution, which was consistent with our initial hypothesis that metal nanoparticle concentrations in the treatments would decrease over time.

Together, these findings support our hypotheses regarding the degradation mechanisms that are caused by photochemical and mechanical stressors and provide insight on the temporal behaviour of metal release from the antifouling paints. Our study provided a foundation for the simultaneous assessment of paint-derived microplastics, metals and metal nanoparticles after exposure to environmental stressors such as UV irradiation and freeze-thaw cycles. Future work should focus on the polymer-specific identification of nanoplastics, temporal sampling for microplastics and the use of complex natural waters to further understand the release behaviour of paint-derived contaminants. Given the inevitability of paint pollution, it is critical to explore the use of sustainable alternatives, reduce paint use and improve paint management practices to

mitigate the pervasive problems stemming from marine paint contamination.

Conflicts of interest

There are no conflicts of interest to declare.

Data availability

Much of the data supporting this article is included as part of the supplementary information (SI). Raw data, in the form of CSV files, and metadata have been deposited in a publicly available repository: https://doi.org/10.5281/zenodo.19672031. Supplementary information: summary of literature examining the release of nanoplastics, microplastics, and metals from various types of paints (Table S1); composition of antifouling paint and primer (Table S2); spectrum of the UV lamp (Fig. S1); supplementary text calculating the equivalent UV irradiation used in the experiment to the real world (Text S1); nujol mull spectrum the suspected rosin (Fig. S2); representative O-PTIR images of antifouling paint microplastics of controls and weathering treatments (Fig. S3); heatmap of Pearson correlation coefficients comparing weathered paint microplastics to reference (Fig. S4); supplementary text explaining low Pearson correlation in CC (Text S2); representative images of coupons for primer paint and antifouling paint after exposure (Fig. S5); representative O-PTIR images of coupons after exposure (Fig. S6); heatmap of Pearson correlation coefficients comparing weathered paint coupons to reference (Fig. S7); contact angles of exposed antifouling paint coupons (Fig. S8); Mann–Whitney *U*-test results comparing the water contact angles (Table S3); average Pearson correlation coefficient of paint microplastics compared to paint coupons (Table S4); heatmap of Pearson correlation coefficients comparing weathered paint microplastics to coupons (Fig. S9); descriptive statistics of particle sizes and particle counts of microscopic images (Table S5); pH measurements for antifouling paint, primer paint, and procedural blanks (Fig. S10); average number concentrations of Cu_2O nanoparticles per gram of dry paint (Fig. S11); representative examples of raw SP-ICP-MS data for Cu_2O (Fig. S12); average mass concentration, average dissolved (ionic) background, and fraction of average mass concentration divided by the average dissolved background of Cu_2O (Table S6). See DOI: https://doi.org/10.1039/d6em00126b.

Acknowledgements

We thank Environment and Climate Change Canada for supporting this project. The work was funded by the Fonds de recherche du Québec Nature et technologies, McGill University, the Advanced Technological Training network on the risk and remediation of Pollution in URban Environments (PURE CREATE), the Natural Sciences and Engineering Research Council of Canada (NSERC), the Centre De Recherche En Écotoxicologie Du Québec (EcotoQ), the Canada Foundation for Innovation and the Canada Research Chairs program. We are grateful to Madjid Hadioui (University of Montreal) for his helpful advice on ICP-MS and SP-ICP-MS analysis, and to Andrew Palucci, Izabela Junqueira Magalhaes, and Elsa Baxter for their assistance in data collection.

References

1 P. Paruta, M. Pucino and J. B. Boucher, in *Plastic Paints the Environment*, 2022.
2 G. Kum, O. Berglund and J. Hollander, Lost in definition: unravelling microplastics from marine coatings through bibliometrics science mapping in thematic analysis and systematic narrative literature review, *Environ. Sci. Eur.*, 2025, **37**, 38.
3 D. M. Yebra, S. Kiil and K. Dam-Johansen, Antifouling technology—past, present and future steps towards efficient and environmentally friendly antifouling coatings, *Prog. Org. Coat.*, 2004, **50**, 75–104.
4 A. S. Adeleye, E. A. Oranu, M. Tao and A. A. Keller, Release and detection of nanosized copper from a commercial antifouling paint, *Water Res.*, 2016, **102**, 374–382.
5 M. Faber, M. Marinković, E. de Valk and S. L. Waaijers-van der Loop, in *Paints and Microplastics*, 2021.
6 Z. T. Diana, Y. Chen and C. M. Rochman, Paint: a ubiquitous yet disregarded piece of the microplastics puzzle, *Environ. Toxicol. Chem.*, 2025, **44**, 26–44.
7 A. Marrion and A. Guy, in *The Chemistry and Physics of Coatings*, ed. A. Marrion, The Royal Society of Chemistry, 2004, p. 50.
8 A. Turner, C. Ostle and M. Wootton, Occurrence and chemical characteristics of microplastic paint flakes in the North Atlantic Ocean, *Sci. Total Environ.*, 2022, **806**, 150375.
9 C. Fang, W. Zhou, J. Hu, C. Wu, J. Niu and R. Naidu, Paint has the potential to release microplastics, nanoplastics, inorganic nanoparticles, and hybrid materials, *Environ. Sci. Eur.*, 2024, **36**, 17.
10 A. Gondikas, K. Mattsson and M. Hassellöv, Methods for the detection and characterization of boat paint microplastics in the marine environment, *Front. Environ. Chem.*, 2023, **4**, DOI: 10.3389/fenvc.2023.1090704.
11 A. L. d. F. Lacerda, L. dos S. Rodrigues, E. van Sebille, F. L. Rodrigues, L. Ribeiro, E. R. Secchi, F. Kessler and M. C. Proietti, Plastics in sea surface waters around the Antarctic Peninsula, *Sci. Rep.*, 2019, **9**, 3977.
12 D.-H. Chae, I.-S. Kim, S.-K. Kim, Y. K. Song and W. J. Shim, Abundance and Distribution Characteristics of Microplastics in Surface Seawaters of the Incheon/Kyeonggi Coastal Region, *Arch. Environ. Contam. Toxicol.*, 2015, **69**, 269–278.
13 J.-H. Kang, O. Y. Kwon, K.-W. Lee, Y. K. Song and W. J. Shim, Marine neustonic microplastics around the southeastern coast of Korea, *Mar. Pollut. Bull.*, 2015, **96**, 304–312.
14 M. F. Mengatto and R. H. Nagai, A first assessment of microplastic abundance in sandy beach sediments of the Paranaguá Estuarine Complex, South Brazil (RAMSAR site), *Mar. Pollut. Bull.*, 2022, **177**, 113530.

15 R. Jaouani, C. Mouneyrac, A. Châtel, F. Amiard, M. Dellali, H. Beyrem, A. Michelet and F. Lagarde, Seasonal and spatial distribution of microplastics in sediments by FTIR imaging throughout a continuum lake - lagoon- beach from the Tunisian coast, *Sci. Total Environ.*, 2022, **838**, 156519.

16 T. Mani, S. Primpke, C. Lorenz, G. Gerdts and P. Burkhardt-Holm, Microplastic Pollution in Benthic Midstream Sediments of the Rhine River, *Environ. Sci. Technol.*, 2019, **53**, 6053–6062.

17 C. Muller-Karanassos, A. Turner, W. Arundel, T. Vance, P. K. Lindeque and M. Cole, Antifouling paint particles in intertidal estuarine sediments from southwest England and their ingestion by the harbour ragworm, Hediste diversicolor, *Environ. Pollut.*, 2019, **249**, 163–170.

18 R. J. Miller, A. S. Adeleye, H. M. Page, L. Kui, H. S. Lenihan and A. A. Keller, Nano and traditional copper and zinc antifouling coatings: metal release and impact on marine sessile invertebrate communities, *J. Nanopart. Res.*, 2020, **22**, 129.

19 T. W. Biggs and H. D'Anna, Rapid increase in copper concentrations in a new marina, San Diego Bay, *Mar. Pollut. Bull.*, 2012, **64**, 627–635.

20 B. Cunha, J. Garnier, D. Araújo, M. Tonhá, C. E. Souto-Oliveira, I. Ruiz, F. H. Feitas e Silva, T. Almeida, R. Freydier, P. Seyler and M. Babinski, Metal record of copper-based antifouling paints in sediment core following marina construction and operation, *Mar. Pollut. Bull.*, 2024, **204**, 116534.

21 W. O. Hobbs, M. McCall, J. Lanksbury, K. Seiders, P. Sandvik, M. Jones, H. Chuhran, D. Momohara and D. Norton, A baseline of copper associated with antifouling paint in marinas within a large fjord estuary, *Mar. Pollut. Bull.*, 2022, **178**, 113547.

22 L. D. F. Costa and M. Wallner-Kersanach, Assessment of the labile fractions of copper and zinc in marinas and port areas in Southern Brazil, *Environ. Monit. Assess.*, 2013, **185**, 6767–6781.

23 K. Schiff, J. Brown, D. Diehl and D. Greenstein, Extent and magnitude of copper contamination in marinas of the San Diego region, California, USA, *Mar. Pollut. Bull.*, 2007, **54**, 322–328.

24 S. Lee, J. Chung and Y.-W. Lee, Cu and Zn Concentrations in Seawater and Marine Sediments Along Korean Coasts from the Perspective of Antifouling Agents, *Bull. Environ. Contam. Toxicol.*, 2018, **101**, 185–190.

25 U.S. Environmental Protection Agency, https://www.epa.gov/wqc/national-recommended-water-quality-criteria-aquatic-life-criteria-table, accessed 10 February 2026.

26 C. Muller-Karanassos, W. Arundel, P. K. Lindeque, T. Vance, A. Turner and M. Cole, Environmental concentrations of antifouling paint particles are toxic to sediment-dwelling invertebrates, *Environ. Pollut.*, 2021, **268**, 115754.

27 S. Soroldoni, S. Vieira da Silva, Í. B. Castro, C. de Martinez Gaspar Martins and G. L. Leães Pinho, Antifouling paint particles cause toxicity to benthic organisms: Effects on two species with different feeding modes, *Chemosphere*, 2020, **238**, 124610.

28 L. Hildebrandt, M. Fischer, O. Klein, T. Zimmermann, F. Fensky, A. Siems, A. Zonderman, E. Hengstmann, T. Kirchgeorg and D. Pröfrock, An analytical strategy for challenging members of the microplastic family: Particles from anti-corrosion coatings, *J. Hazard. Mater.*, 2024, **470**, 134173.

29 I. Omae, Organotin antifouling paints and their alternatives, *Appl. Organomet. Chem.*, 2003, **17**, 81–105.

30 M. Simon, A. Vianello, Y. Shashoua and J. Vollertsen, Accelerated weathering affects the chemical and physical properties of marine antifouling paint microplastics and their identification by ATR-FTIR spectroscopy, *Chemosphere*, 2021, **274**, 129749.

31 N. Singh and A. Turner, Leaching of copper and zinc from spent antifouling paint particles, *Environ. Pollut.*, 2009, **157**, 371–376.

32 A. Jalaie, A. Afshaar, S. B. Mousavi and M. Heidari, Investigation of the Release Rate of Biocide and Corrosion Resistance of Vinyl-, Acrylic-, and Epoxy-Based Antifouling Paints on Steel in Marine Infrastructures, *Polymers*, 2023, **15**, 3948.

33 E. Ytreberg, J. Karlsson and B. Eklund, Comparison of toxicity and release rates of Cu and Zn from anti-fouling paints leached in natural and artificial brackish seawater, *Sci. Total Environ.*, 2010, **408**, 2459–2466.

34 M. A. Bighiu, E. Gorokhova, B. Carney Almroth and A.-K. Eriksson Wiklund, Metal contamination in harbours impacts life-history traits and metallothionein levels in snails, *PLoS One*, 2017, **12**, e0180157.

35 A. Katranitsas, J. Castritsi-Catharios and G. Persoone, The effects of a copper-based antifouling paint on mortality and enzymatic activity of a non-target marine organism, *Mar. Pollut. Bull.*, 2003, **46**, 1491–1494.

36 K. B. Adhikary, S. Pang and M. P. Staiger, Effects of the accelerated freeze-thaw cycling on physical and mechanical properties of wood flour-recycled thermoplastic composites, *Polym. Compos.*, 2010, **31**, 185–194.

37 A. Azimzada, J. M. Farner, M. Hadioui, C. Liu-Kang, I. Jreije, N. Tufenkji and K. J. Wilkinson, Release of TiO 2 nanoparticles from painted surfaces in cold climates: characterization using a high sensitivity single-particle ICP-MS, *Environ. Sci. Nano*, 2020, **7**, 139–148.

38 ASTM D3623-78a, *Test Method for Testing Antifouling Panels in Shallow Submergence*, ASTM International, 1998, preprint, DOI: 10.1520/D3623-78AR98.

39 ASTM D6442-06, *Test Method for Determination of Copper Release Rate From Antifouling Coatings in Substitute Ocean Water*, ASTM International, 2020, preprint, DOI: 10.1520/D6442-06R20.

40 L. M. Hernandez, J. Grant, P. S. Fard, J. M. Farner and N. Tufenkji, Analysis of ultraviolet and thermal degradations of four common microplastics and evidence of nanoparticle release, *J. Hazard. Mater. Lett.*, 2023, **4**, 100078.

41 T. E. Lockwood, L. Schlatt and D. Clases, SPCal – an open source, easy-to-use processing platform for ICP-TOFMS-based single event data, *J. Anal. At. Spectrom.*, 2025, **40**, 130–136.
42 N. Abd Rashid, Y. S. Salim, S. I. Abdul Halim, M. K. Harun, C. H. Ong and C. H. Chan, FTIR conformity analysis and performance testings of fresh, aged and expired polymeric paints under different storage conditions, *Pure Appl. Chem.*, 2023, **95**, 81–98.
43 S. Primpke, R. K. Cross, S. M. Mintenig, M. Simon, A. Vianello, G. Gerdts and J. Vollertsen, Toward the Systematic Identification of Microplastics in the Environment: Evaluation of a New Independent Software Tool (siMPle) for Spectroscopic Analysis, *Appl. Spectrosc.*, 2020, **74**, 1127–1138.
44 L. Holmes and A. Turner, Leaching of hydrophobic Cu and Zn from discarded marine antifouling paint residues: Evidence for transchelation of metal pyrithiones, *Environ. Pollut.*, 2009, **157**, 3440–3444.
45 A. Jessop and A. Turner, Leaching of Cu and Zn from discarded boat paint particles into tap water and rain water, *Chemosphere*, 2011, **83**, 1575–1580.
46 Y.-J. An and D. H. Kampbell, Total, dissolved, and bioavailable metals at Lake Texoma marinas, *Environ. Pollut.*, 2003, **122**, 253–259.
47 S. Melaku, R. Dams and L. Moens, Determination of trace elements in agricultural soil samples by inductively coupled plasma-mass spectrometry: Microwave acid digestion versus aqua regia extraction, *Anal. Chim. Acta*, 2005, **543**, 117–123.
48 P. A. Hayes, S. Vahur and I. Leito, ATR-FTIR spectroscopy and quantitative multivariate analysis of paints and coating materials, *Spectrochim. Acta, Part A Mol. Biomol. Spectrosc.*, 2014, **133**, 207–213.
49 J. van der Weerd, A. van Loon and J. J. Boon, FTIR Studies of the Effects of Pigments on the Aging of Oil, *Stud. Conserv.*, 2005, **50**, 3–22.
50 K. Gotoh, Y. Nakata, M. Tagawa and M. Tagawa, Wettability of ultraviolet excimer-exposed PE, PI and PTFE films determined by the contact angle measurements, *Colloids Surf., A*, 2003, **224**, 165–173.
51 M. González-Cabrera, A. Domínguez-Vidal and M. J. Ayora-Cañada, Monitoring UV-accelerated alteration processes of paintings by means of hyperspectral micro-FTIR imaging and chemometrics, *Spectrochim. Acta, Part A Mol. Biomol. Spectrosc.*, 2021, **253**, 119568.
52 C. Azémard, C. Vieillescazes and M. Ménager, Effect of photodegradation on the identification of natural varnishes by FT-IR spectroscopy, *Microchem. J.*, 2014, **112**, 137–149.
53 Y. Kang, H. H. Jo and S. Kim, Effects of UV degradation on building materials with emphasis on microplastic generation potential, *J. Hazard. Mater.*, 2025, **483**, 136521.
54 S. Jacobsen, G. W. Scherer and E. M. Schulson, Concrete–ice abrasion mechanics, *Cem. Concr. Res.*, 2015, **73**, 79–95.
55 M. Thomas, in *Marine Concrete Structures*, Elsevier, 2016, pp. 151–170.
56 A. Turner, Paint particles in the marine environment: An overlooked component of microplastics, *Water Res.:X*, 2021, **12**, 100110.
57 A. Turner, S. Comber, A. B. Rees, D. Gkiokas and K. Solman, Metals in boat paint fragments from slipways, repair facilities and abandoned vessels: An evaluation using field portable XRF, *Talanta*, 2015, **131**, 372–378.
58 A. Turner, Marine pollution from antifouling paint particles, *Mar. Pollut. Bull.*, 2010, **60**, 159–171.
59 D. M. Yebra, S. Kiil, C. E. Weinell and K. Dam-Johansen, Dissolution rate measurements of sea water soluble pigments for antifouling paints: ZnO, *Prog. Org. Coat.*, 2006, **56**, 327–337.
60 L. Fréchette-Viens, M. Hadioui and K. J. Wilkinson, Quantification of ZnO nanoparticles and other Zn containing colloids in natural waters using a high sensitivity single particle ICP-MS, *Talanta*, 2019, **200**, 156–162.
61 M. Hadioui, C. Peyrot and K. J. Wilkinson, Improvements to Single Particle ICPMS by the Online Coupling of Ion Exchange Resins, *Anal. Chem.*, 2014, **86**, 4668–4674.
62 P. Pfohl, K. Santizo, J. Sipe, M. Wiesner, S. Harrison, C. Svendsen and W. Wohlleben, Environmental degradation and fragmentation of microplastics: dependence on polymer type, humidity, UV dose and temperature, *Microplast. Nanoplast.*, 2025, **5**, 7.
63 E. R. Silva and G. Jiang, The Hidden Threats of Biofouling and Microbiologically Influenced Corrosion—Implications for Coatings Science and Sustainable Infrastructure, *Coatings*, 2026, **16**, 123.
64 M. Mutschlechner, R. Gstir, H. Schöbel, A. Rössler, C. Lass-Flörl and K. Bach, From process to product: exploring microbial diversity in paints, *J. Coat. Technol. Res.*, 2025, **22**, 481–490.